E field by changing the frequency between low (10 Hz) and high (10,000 Hz) values while the material was curing. The direction of the nematic director could be rotated from homeotropic (perpendicular to film plane) to planar (parallel to film plane) alignment with respect to the electrode surface; that is, at low frequencies, we observed mesogens oriented parallel to the *E* field, but at high frequencies, the compound changed its director by 90°. Compared to known low–molecular weight compounds with similar structure, we expect the crossover frequency at 190°C to be on the order of 5000 Hz, but detailed dielectric measurements during curing have yet to be carried out to clarify this question.

13. At 190°C, DCN cures within 3 hours, and at 250°C, in 30 min, forming a densely cross-linked structure.
14. The calculations were carried out with the appropriate corrections for uniaxially oriented fibers after background correction. The *d* spacings from wide-angle XRD data were 5.2 Å for DCN and 4.8 Å for CHDCN.
15. In contrast, the radial width of the reflections, which can approximately describe the order of the nematic phase, shows a higher order for CHDCN than for DCN, where the wide-angle reflections are unusually broad along the radial direction. The radial width of a reflection offers information about the domain size of the nematic phase of a polymer. Although the orientation for CHDCN is weaker, its domain size is larger than that for DCN.
16. We thank the Cornell Materials Science Center and the National Science Foundation (DMR-9321573) for partial support of this work. Support for H.K. from the Industry-Cornell Alliance for Electronic Packaging, the Fulbright Foundation, and the Laser Hardened Materials Branch of Wright-Patterson Air Force Base is appreciated. Support for T.J.B. under Air Force contract F33615-95-C-5423 is acknowledged. Helpful discussions with W. Adams and E. J. Kramer are gratefully acknowledged. Access to the Cornell High Energy Synchrotron was essential for this work.

14 November 1995; accepted 25 January 1996

Imaging and Time-Resolved Spectroscopy of Single Molecules at an Interface

J. J. Macklin,* J. K. Trautman,* T. D. Harris, L. E. Brus

Far-field microscopy was used to noninvasively measure the room-temperature optical properties of single dye molecules located on a polymer-air interface. Shifts in the fluorescence spectrum, due to perturbation by the locally varying molecular environment, and the orientation of the transition dipole moment were correlated to variation in the excited-state lifetime. The lifetime dependence on spectral shift is argued to result from the frequency dependence of the spontaneous emission rate; the lifetime dependence on dipole orientation was found to be a consequence of the electromagnetic boundary conditions on the fluorescent radiation at the polymer-air interface.

Optical spectroscopy of single molecules can reveal the variation in molecular environments normally averaged over in ensemble measurements. A molecular emission spectrum and excited-state lifetime, perturbed by local fields and neighboring dipoles, can be a sensitive microscopic probe of chemical and biological processes, particularly if correlated to molecular location and orientation. High-resolution spectroscopy of single impurity molecules in bulk media has been obtained at cryogenic temperatures (*1–5*), and at room temperature, near-field microscopy has been used to study spatially resolved molecules at surfaces (*6–10*). However, the near-field method requires proximity of a molecule to a metallized near-field probe, which can perturb the molecular properties under study (*8–10*). Noninvasive far-field illumination of single molecules in liquids (*11*) and surfaces (*12*) has recently been reported, but far-field room-temperature spectroscopy has not been done. In the present study the location, orientation, fluorescence lifetime, and spectrum of single carbocyanine dye molecules at a polymer-air interface were measured by far-field microscopy. The method is not limited to molecules at a surface, allowing quantitative comparison with molecules in bulk media. On the basis of such a comparison, the dependence of the excited-state lifetime on spectral shifts and on dipole orientation was determined.

We obtained fluorescence images and spectral measurements of single molecules in an epi-illumination scanning microscope using a focused 532-nm laser beam for excitation (*13*). In the imaging we used raster-scanning of a sample across the focused laser spot; we performed spectroscopy by positioning and holding one molecule at a time under laser illumination. The samples consisted of randomly oriented carbocyanine dye molecules, $DiIC_{12}(3)$ (*14*), in a polymethylmethacrylate (PMMA) film 20-nm thick on a quartz cover slip (*15*), prepared by spin-coating so that the areal density was one to five molecules per square micrometer. At this low coverage, molecules could be easily resolved spatially. Measurements were made at an excitation laser intensity of ~500 W cm^{-2}, well below the saturation intensity of 10 kW cm^{-2} (*16*).

Fluorescence images were used to locate molecules immobilized in the PMMA film (Fig. 1). Next, polarized excitation with unpolarized-fluorescence detection was used to determine the component of the absorption transition dipole in the plane of the sample (the *x*–*y* plane in Fig. 1). For an absorption dipole oriented with polar and azimuthal angles of θ_a and ϕ_a, respectively, illuminated with laser light polarized in the *x*–*y* plane at an angle ϕ_L from the *x* axis, the detected fluorescence rate *R* is

$$R(\phi_L) = R_0 \sin^2\theta_a \cos^2(\phi_a - \phi_L) \quad (1)$$

where R_0 is the detected fluorescence rate for a molecule aligned entirely along the polarization axis of the laser field (*17*). By rotating the laser polarization from $\phi_L = 0$ to $\phi_L = 90°$, we found that the azimuthal orientation of molecules a to d was along the *x* axis ($\phi_a = 0$), molecules e to i along the *y* axis, and molecules j and k at about $\phi_a = 45°$. The polar angle θ_a, and hence the *z* component of the absorption dipole, cannot be measured directly here because the *z* component of the laser field is too small (*18*). The polar orientation can be estimated from Eq. 1 if ϕ_a is measured and the maximum fluorescence rate R_0 is known or estimated. Molecular orientation, and in particular the emission dipole [which is not collinear with the absorption dipole for $DiIC_{12}(3)$ (*19*)], can significantly affect the excited-state lifetime of a molecule near an interface.

Time-resolved spectroscopy (Fig. 2) was attempted on more than 200 molecules, of which about 30% survived irreversible photobleaching for a sufficient period to allow a measurement with good counting statistics. Molecules were characterized by their excited-state lifetime τ and their peak fluorescence wavelength λ_p, both of which varied from molecule to molecule. On the basis of 68 single-molecule measurements, a distribution of fluorescence lifetimes (Fig. 3A) and peak wavelengths (Fig. 3B) and the correlation of lifetime with peak wavelength (Fig. 3C) were determined. The mean values of τ and λ_p were 2.67 ns and 565 nm, respectively, in agreement with an ensemble measurement of $\tau = 2.7$ ns and $\lambda_p = 565$ nm shown in Fig. 2. However, the dispersion and correlation of these spectral properties, which we discuss below, could not be obtained from an ensemble measurement.

First, the peak fluorescence wavelength shifted by up to 30 nm, and the distribution had a width of 8 nm, or 30 meV, which is slightly larger than the thermal energy at room temperature. These spectral shifts, consistent with those observed with the use of near-field spectroscopy (*7*), are attributed to variation in the local PMMA environment. The PMMA polymer is polar and polarizable, whereas $DiIC_{12}(3)$ has a large excited-state polarizibility. The perturbed molecular transition energies and hence the wavelength of the

AT&T Bell Laboratories, Murray Hill, NJ 07974, USA.

*To whom correspondence should be addressed.

fluorescence emission are sensitive probes of the locally varying environment. In addition to the observed spectral shifts, about 10% of the molecules exhibited a redistribution in the intensity of the spectral components, as compared with the average spectrum.

Second, the fluorescence lifetime varied by greater than 50% and exhibited a trend of increasing duration for molecules with red-shifted spectra (Fig. 3C). If the lifetime is purely radiative, this wavelength-dependent trend can be understood as follows. The total radiative rate is the sum of the rates for the individual vibronic transitions that make up the emission spectrum, each of which is proportional to $|\mu_{ul}|^2\ \omega^3_{ul}$, where μ_{ul} is the dipole matrix element between the upper (u) and lower (l) states at emission frequency ω_{ul}. For a broad spectrum, the total radiative lifetime is approximately (*20*) proportional to the cube of the peak fluorescence wavelength, $(\lambda_p)^3$. If the dipole matrix elements μ_{ul} are independent of the environmentally induced perturbation that shifts the transition energies, then molecules with red-shifted peak wavelengths will have longer lifetimes that increase as $(\lambda_p)^3$. A small nonradiative rate would not substantially alter this result.

A cubic dependence on peak wavelength cannot be responsible for the fact that molecules with indistinguishable fluorescence spectra had lifetimes that varied by up to 50%. However, this large variation can arise for a molecule near a dielectric interface, which modifies the radiative component of the excited-state lifetime because of the boundary conditions imposed on the radiated field (*21*):

$$\frac{1}{\tau} = \frac{1}{\tau_{nr}} + \frac{1}{\tau_{rad}} \times \left[\frac{L_{\parallel}(z)}{L_{\infty}} \sin^2\theta_e + \frac{L_{\perp}(z)}{L_{\infty}} \cos^2\theta_e\right] \quad (2)$$

where $1/\tau_{nr}$ and $1/\tau_{rad}$ are the nonradiative and radiative rates, respectively. The quantity in brackets accounts for the proximity of a molecule to the PMMA-air dielectric interface; this quantity depends on the polar orientation of the emission dipole, θ_e; the distance, z, of the molecule from the interface (negligible here); and the ratio of refractive indices of the dielectrics constituting the interface. Algebraic expressions for the normalized radiated powers $L_{\parallel}/L_{\infty}$ and $L_{\perp}/L_{\infty}$ are given in (*21*); for a PMMA-air interface, they are 0.92 and 0.34, respectively. Thus, a molecule with a perpendicularly oriented emission dipole should have a lifetime 2.7 times that of a molecule oriented parallel to the interface (*22*). If a molecule is moved far from the interface (farther than a few optical wavelengths) or if the refractive index difference of the interface is reduced to zero, both $L_{\parallel}/L_{\infty}$ and $L_{\perp}/L_{\infty}$ approach unity, and the lifetime is independent of orientation. The quantum yield, defined as $\Phi_F = 1 - (\tau/\tau_{nr})$, also depends on the emission-dipole orientation through Eq. 2.

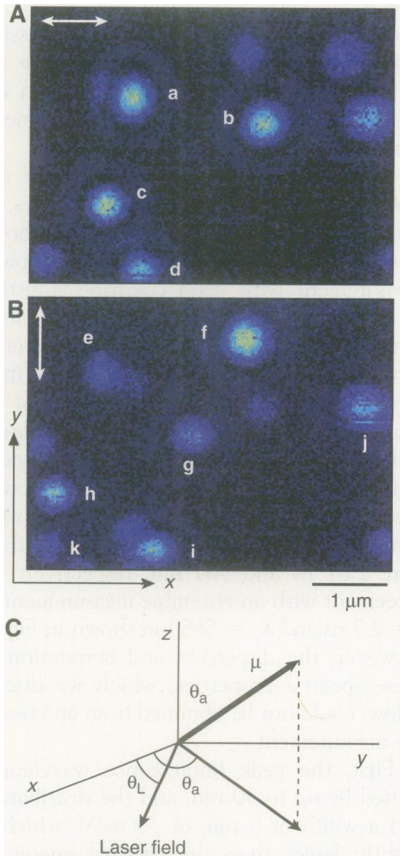

Fig. 1. Sequential fluorescence images (**A**) and (**B**) of the same sample area showing single dye molecules at a PMMA-air interface, taken with 532-nm laser excitation polarized as indicated by the arrows. The brightest molecules had count rates of 280 counts per pixel (1 pixel = 10 ms) and a signal-to-background ratio of 30:1. (**C**) Geometry used in Eq. 1 to determine the orientation of the absorption dipole moment in the *x*–*y* plane.

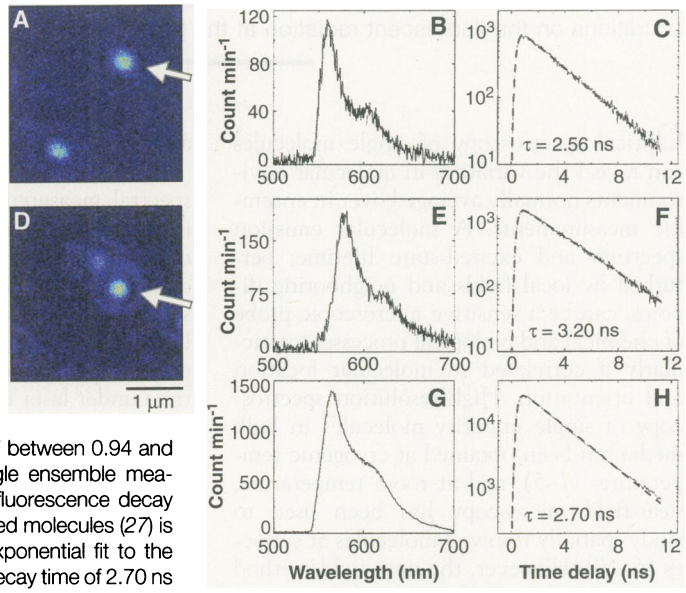

Fig. 2. Fluorescence images (**A** and **D**), corresponding spectra (**B** and **E**), and fluorescence decays (**C** and **F**) for two molecules located at a PMMA-air interface. The peak emission wavelength λ_p was 560 nm in (B) and 578 nm in (E). Lifetimes were fit to a single exponential (dotted curves), with 1/*e* decay times of 2.56 ns (χ^2 = 1.05) in (C) and 3.20 ns (χ^2 = 1.16) in (F). Other single-molecule lifetimes yielded unbiased, shot-limited residuals with χ^2 between 0.94 and 1.4. For comparison, a single ensemble measurement of spectrum and fluorescence decay averaged over several hundred molecules (*27*) is shown in (**G**) and (**H**). An exponential fit to the ensemble lifetime yielded a decay time of 2.70 ns (χ^2 = 6.7). This χ^2 is indicative of a large deviation from single-exponential behavior, reflecting the ensemble average over a distribution of lifetimes.

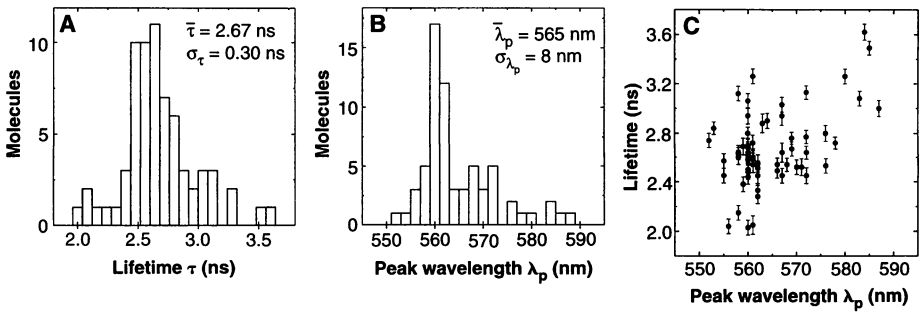

Fig. 3. Distribution of (**A**) lifetime τ and (**B**) peak fluorescence wavelength λ_p and the correlation (**C**) of lifetime with peak wavelength for 68 molecules at a PMMA-air interface. Mean lifetime $\bar{\tau}$ was 2.67 ns (standard deviation, σ_τ, of 0.30 ns) and mean peak wavelength $\bar{\lambda}_p$ was 565 nm (σ_{λ_p} = 8 nm). Error bars in (C) reflect the uncertainty in the measured lifetime, determined by changing the fitted lifetime until χ^2 increased by one (*28*).

To test the effect of the interface, we performed an experiment that reduced the dielectric contrast of the interface while preserving the orientational distribution of molecules spin-coated on the PMMA film. A sample was prepared as described above and then coated with either a drop of index-matching fluid (refractive index n = 1.48) (*23*) or with several micrometers of PMMA (n = 1.48) (*24*). In both cases, the refractive index difference of the interface was reduced from 0.48 to less than 0.02. Fluorescence decays and spectra were obtained as before for 31 individual molecules on an oil-covered sample and for an additional 31 molecules on a PMMA-covered sample.

In the correlation plot of τ versus λ_p for these molecules (Fig. 4A), it is apparent that the scatter in lifetime is significantly reduced even though the spectral shifts are nearly as large as before, with no systematic difference in lifetime between the oil- and the PMMA-overcoated samples. The small residual decay rate, possibly due to an environmentally induced perturbation of the intramolecular matrix elements, varied from molecule to molecule by less than 1/20 ns^{-1}. In addition, this set of measurements appears to have a wavelength-dependent upper bound on lifetime. Assuming that the lifetime was radiative and varied as the cube of the peak wavelength, a fit to the upper bound is given by $\tau_{rad} = 2.57(\lambda_p/565)^3$ and is plotted in Fig. 4A. A radiative lifetime of 2.57 ns in PMMA at a peak wavelength of 565 nm agrees with that found (τ_{rad} = 2.84 ns in ethanol, λ_p = 565 nm) for the short-chain analog $DiIC_2(3)$ (*25*).

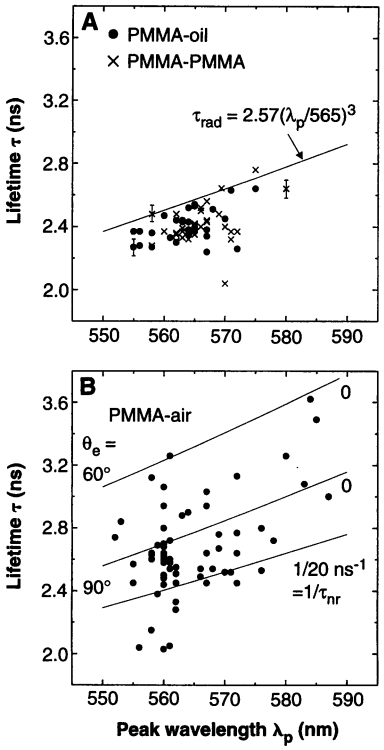

Fig. 4. (**A**) Fluorescence lifetime versus peak emission wavelength for molecules spin-coated on PMMA and overcoated with several micrometers of either a hydrocarbon immersion oil (circles) or PMMA (crosses), both of which reduce the refractive index difference of the interface to less than 0.02. Representative error bars are shown. The solid line is an approximation to the maximum observed lifetime. (**B**) The data of Fig. 3C are replotted; the solid lines are the calculated lifetimes (Eq. 2) for different polar orientations θ_e and nonradiative decay rates $1/\tau_{nr}$ of the emission dipole.

Using this wavelength-dependent radiative lifetime in Eq. 2, we plotted the calculated τ for a molecule located at the PMMA-air interface in Fig. 4B for an emission dipole oriented (i) parallel to the surface (θ_e = 90°), (ii) tilted with θ_e = 60° from the surface normal, and (iii) parallel to the surface with a nonradiative rate of $1/\tau_{rad}$ of 1/20 ns^{-1}. Comparison to the experimental data shows that the measured fluorescence lifetimes are consistent with emission dipoles tilted by 90° to 60° from the surface normal. Short fluorescence lifetimes can be accounted for by a nonradiative decay rate less than 1/20 ns^{-1}. Very long lifetimes, expected for molecules nearly perpendicular to the surface, were not observed in this set of measurements.

To test whether long lifetimes occur, lifetime and spectrum measurements were made on molecules at the PMMA-air interface with very different fluorescence rates, but with the same azimuthal angle and peak emission wavelength. Identical excitation and collection conditions allowed accurate determination of the relative fluorescence rate. Significantly longer fluorescent lifetimes were observed for molecules with low fluorescence rates (Fig. 5). If the quantum yield and cross section are approximately constant, then according to Eq. 1 a small fluorescence rate is indicative of a molecule having an absorption transition dipole with a large z component. The interface thus produced a large modification of the excited-state lifetime. Molecular orientation can thus be established by using the relative fluorescence rate to estimate the z component of the absorption dipole and by using the lifetime to estimate the orientation of the emission dipole (inset to Fig. 5).

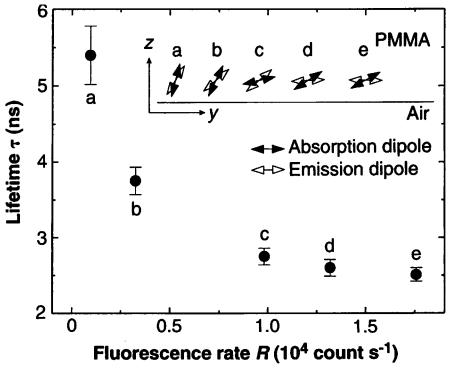

Fig. 5. Measured lifetime versus fluorescence rate for molecules with the same azimuthal orientation (ϕ_a = 90°) of the absorption dipole and with a peak wavelength of 560 nm. Inset shows polar orientation of the absorption (θ_a) and emission (θ_e) dipoles determined from the fluorescence intensity (Eq. 1, with $R_0 = 2 \times 10^4$ count s^{-1} based on the brightest molecules observed under these conditions) and from lifetime (Eq. 2), respectively.

It would in principle be possible to use a higher order spatial beam profile, which at the focus of a high numerical aperture optic would have a substantial longitudinal electric field (*26*). This would allow direct measurement of all three components of the absorption transition-dipole moment.

REFERENCES AND NOTES

1. W. P. Ambrose, T. Basche, W. E. Moerner, *J. Chem. Phys.* **95**, 7150 (1991).
2. T. Basche, W. E. Moerner, M. Orrit, H. Talon, *Phys. Rev. Lett.* **69**, 1516 (1992).
3. P. Tchenio, A. B. Myers, W. E. Moerner, *Chem. Phys. Lett.* **213**, 325 (1993).
4. A. Zumbusch, L. Fleury, R. Brown, J. Bernard, M. Orrit, *Phys. Rev. Lett.* **70**, 3584 (1993); J. Bernard, L. Fleury, H. Talon, M. Orrit, *J. Chem. Phys.* **98**, 850 (1993).
5. F. Guttler *et al.*, *J. Lumin.* **56**, 29 (1993).
6. E. Betzig and R. J. Chichester, *Science* **262**, 1422 (1993).
7. J. K. Trautman, J. J. Macklin, L. E. Brus, E. Betzig; *Nature* **369**, 40 (1994).
8. X. Sunney Xie and R. C. Dunn, *Science* **265**, 361 (1994).
9. W. P. Ambrose, P. M. Goodwin, J. C. Martin, R. A. Keller, *ibid.*, p. 364.
10. J. K. Trautman and J. J. Macklin, *Chem. Phys.*, in press.
11. S. Nie, D. T. Chiu, R. N. Zare, *Science* **266**, 1018 (1994).
12. T. Funatsu, Y. Harada, M. Tokunaga, K. Saito, T. Yanagida, *Nature* **374**, 555 (1995).
13. Mode-locked 532-nm laser pulses were focused onto a sample of molecules by an oil-immersion objective that collected the fluorescence. The objective was used at its full numerical aperture (NA) of 1.25 for collecting fluorescence and at 0.82 NA for focusing the laser. The laser spot size, typically 0.38 μm full width at half maximum, determined the spatial resolution. To produce a fluorescence image, we mounted the sample on a piezoelectric tube and raster-scanned it across the focused laser spot. Unpolarized fluorescence collected by the oil-immersion objective was focused onto an avalanche photodiode detector. Detector photocounts and the x–y scan voltages were digitized to construct an image. To perform spectroscopy, we used the piezoelectric tube to position a molecule under the focused laser spot, and a beam splitter was inserted to send 80% of the fluorescence to a spectrometer and 14% to the avalanche photodiode. Time-correlated photon counting was used to determine the fluorescence decay. Spectrum and lifetime were thus obtained simultaneously. Spectra were corrected for transmission through the dichroic optics. For each fluorescent decay, ~10^5 counts were recorded during 1-min measurement intervals. Background acquired after a molecule photobleached was typically 10^3 counts and was subtracted out of the data.
14. $DiIC_{12}(3)$ is 1,1′-didodecyl-3,3,3′,3′-tetramethylindocarbocyanine, catalog no. D-383, Molecular

Probes. These molecules have low photobleaching rates (10^{-6} to 10^{-8} per excitation), near-unity quantum yield in a semirigid environment, and an absorption cross section of 1.35×10^{-16} cm^2 at 532 nm, estimated by us on the basis of the measured absorption in methanol.
15. A quartz cover slip was first spin-coated with one drop (0.2 ml) of 0.1% by weight PMMA in chlorobenzene and then spin-coated with one drop of a 1-nM solution of $DiI_{12}C(12)$ in toluene. The nanomolar dye solution was freshly prepared from a micromolar dye solution with each sample.
16. Although the calculated saturation intensity is 1 MW cm^{-2}, in a separate study we found that the saturation of the fluorescent transition was determined by transitions from the excited singlet state to a metastable state, probably the triplet state, with an intersystem crossing rate of about 0.15% and a triplet lifetime of 0.4 ms.
17. The maximum fluorescence rate is $R_0 = \eta \Phi_F(\sigma I/h\nu)$, where σ is the absorption cross section at the laser frequency ν, Φ_F is the fluorescence quantum yield, I is the laser intensity, and η is the collection efficiency. In general, both η and Φ_F can depend on the emission dipole orientation. However, the 1.25-NA oil-immersion objective used here collected a calculated 65% of the total light emitted by a molecule at the PMMA-air interface [E. H. Helen and D. Axelrod, *J. Opt. Soc. Am. B* **4**, 337 (1987)], nearly independent of the emission-dipole orientation. The total collection or detection efficiency was 15%.
18. A focused laser beam has a very small longitudinal field component along the z axis, on the order of E/kw, where E is the tangential laser field, k is $2\pi/\lambda$, and w is the focused spot size [M. Lax, W. H. Louisell, W. B. McKnight, *Phys. Rev. A* **11**, 1365 (1975)].
19. The emission dipole, which lies along the long axis of the molecule that connects the two indole rings, is oriented 28° from the absorption dipole [D. Axelrod, *Biophys. J.* **26**, 557 (1979)].
20. The radiative lifetime for a broad molecular spectrum is proportional to the spectrally averaged inverse cube of the emission frequency [S. J. Strickler and R. A. Berg, *J. Chem. Phys.* **37**, 814 (1962)] or, to a small approximation, proportional to the cube of the peak fluorescence wavelength.
21. W. Lukosz and R. E. Kunz, *Opt. Commun.* **20**, 195 (1977); *J. Opt. Soc. Am.* **67**, 1607 (1977).
22. For a dipole on the air side of the interface, $L_{\|}/L_{\infty}$ is 0.92, $L_{\perp}/L_{\infty}$ is 1.6, and the radiative lifetime is decreased for a perpendicular emission dipole.
23. Aliphatic hydrocarbon immersion oil, type FF; Cargille Laboratories, Cedar Grove, NJ.
24. We deposited several micrometers of PMMA by spin-coating several drops of a solution of 5% by weight PMMA in toluene and heating the sample to dry.
25. E. Akesson, V. Sundstrom, T. Gillbro, *Chem. Phys. Lett.* **121**, 513 (1985).
26. M. O. Scully, *Appl. Phys. B* **51**, 238 (1990).
27. We obtained an ensemble measurement by raster-scanning a 36-μm^2 sample area prepared with 20 times higher coverage of molecules at a laser intensity of 500 W cm^{-2}, while continuously collecting fluorescence. It thus averaged over several hundred molecules.
28. P. R. Bevington, *Data Reduction and Error Analysis for the Physical Sciences* (McGraw-Hill, New York, 1969), chap. 11.

26 October 1995; accepted 19 January 1996

Positional Cloning of the Werner's Syndrome Gene

Chang-En Yu,* Junko Oshima,* Ying-Hui Fu,* Ellen M. Wijsman, Fuki Hisama, Reid Alisch, Shellie Matthews, Jun Nakura, Tetsuro Miki, Samir Ouais, George M. Martin, John Mulligan, Gerard D. Schellenberg†

Werner's syndrome (WS) is an inherited disease with clinical symptoms resembling premature aging. Early susceptibility to a number of major age-related diseases is a key feature of this disorder. The gene responsible for WS (known as *WRN*) was identified by positional cloning. The predicted protein is 1432 amino acids in length and shows significant similarity to DNA helicases. Four mutations in WS patients were identified. Two of the mutations are splice-junction mutations, with the predicted result being the exclusion of exons from the final messenger RNA. One of these mutations, which results in a frameshift and a predicted truncated protein, was found in the homozygous state in 60 percent of Japanese WS patients examined. The other two mutations are nonsense mutations. The identification of a mutated putative helicase as the gene product of the WS gene suggests that defective DNA metabolism is involved in the complex process of aging in WS patients.

Werner's syndrome is a rare autosomal recessive disorder that is considered a partial model of human aging (*1–3*). WS patients prematurely develop a variety of the major age-related diseases, including several forms of arteriosclerosis, malignant neoplasms, type II diabetes mellitus, osteoporosis, and ocular cataracts; these individuals also manifest early graying and loss of hair, skin atrophy, and a generally aged appearance. Growth retardation occurs, typically around the time of puberty, but medical problems are rare during childhood. Cell culture studies also suggest a parallel between WS and aging; the replicative life-span of fibroblasts from WS patients is reduced compared with age-matched controls and is similar to the life-span of fibroblasts taken from more elderly individuals (*4*). However, some prevalent geriatric disorders such as Alzheimer's disease and hypertension are not observed in WS. Moreover, there are subtle discordances between WS and normal aging, such as a disproportionately severe osteoporosis of the limbs relative to the trunk and the high prevalence of nonepithelial neoplasms in WS. Finally, there are unusual clinical features unrelated to aging, including ulcerations around the ankles and soft tissue calcification (*1*, *2*).

The WS locus (*WRN*) was initially localized to 8p12 (*5*) by linkage analysis and the genetic position refined by both meiotic and homozygosity mapping (*5–7*). Initial mapping (*6–8*) placed *WRN* in an 8.3-centimorgan (cM) interval flanked by markers D8S137 and D8S87 (Fig. 1); D8S339, located within this interval, was the closest marker. Subsequently, short tandem repeat polymorphism (STRP) markers at the glutathione reductase (*GSR*) gene and D8S339 were shown to be in linkage disequilibrium with WS in Japanese WS patients (*9*, *10*), indicating that these markers are most likely close to *WRN*.

To clone the WS gene, we generated a map from yeast artificial chromosomes (YACs), P1 clones, and cosmid contigs (Fig. 1), starting at *GSR* and extended by walking methods to cover approximately 3 Mb (*11*). Eighteen STRP markers (Fig. 1B) were identified in the contig; probable recombinants were detected at D8S2194 (which excluded the region telomeric to this marker) and at D8S2186 [which excluded the region centromeric to this marker (*12*)], making the 1.2 to 1.4 Mb interval

C.-E. Yu and S. Matthews, Geriatric Research Education and Clinical Center (182B), Veterans Affairs Puget Sound Health Care System, Seattle Division, 1660 South Columbian Way, Seattle, WA 98108, USA, and Department of Neurology, University of Washington, Seattle, WA 98195, USA.
J. Oshima, Geriatric Research Education and Clinical Center (182B), Veterans Affairs Puget Sound Health Care System, Seattle Division, 1660 South Columbian Way, Seattle, WA 98108, USA, and Department of Pathology, University of Washington, Seattle, WA 98195, USA.
Y.-H. Fu, R. Alisch, J. Mulligan, Darwin Molecular Corporation, 1631 220th Street, S.E., Bothell, WA 98021, USA.
E. M. Wijsman, Division of Medical Genetics, Department of Medicine, and Department of Biostatistics, University of Washington, Seattle, WA 98195, USA.
F. Hisama, Department of Neurology, Yale University School of Medicine, New Haven, CT 06510, USA.
J. Nakura and T. Miki, Department of Geriatric Medicine, Osaka University Medical School, 2-2 Yamadaoka Suita, Osaka 565, Japan.
S. Ouais, Section of Endocrinology, Damascus City Hospital, Damascus, Syria.
G. M. Martin, Department of Pathology, University of Washington, Seattle, WA 98195, USA.
G. D. Schellenberg, Geriatric Research Education and Clinical Center (182B), Veterans Affairs Puget Sound Health Care System, Seattle Division, 1660 South Columbian Way, Seattle, WA 98108, USA, and the Departments of Medicine, Neurology, and Pharmacology, University of Washington, Seattle, WA 98195, USA.
*These authors contributed equally to this work.
†To whom correspondence should be addressed.